Neural Network Modeling for the Reduction of Scattering Grating Lobes of Arrays

Zhi-Xian Liu[1], Wen-Hao Su[1], Sheng-Jun Zhang[2], and Wei Shao[1]

[1]School of Physics
University of Electronic Science and Technology of China
Chengdu, China
zxliu@std.uestc.edu.cn, suwenhao1202@163.com, weishao@uestc.edu.cn

[2]National Key Laboratory of Science and Technology on Test Physics and Numerical Mathematics
Beijing 100076, China
zhangsj98@sina.com

***Abstract* –** The monostatic radar cross-section (RCS) of an array is seriously deteriorated by the scattering grating lobe. In this paper, the scattering grating lobe of an array is suppressed by metal walls around elements. The artificial neural network with Fourier series-based transfer functions is used to accelerate the design process. A 1×8 array with the patch element operating in the range from 9.4 to 10.6 GHz is studied. The monostatic RCS of the array with designed metal walls is compared with that of the array with no metal wall. Simulated results show that the scattering grating lobe of the array with metal walls is suppressed by 5.8 dB at 12 GHz, and the change of radiation performance is acceptable. The design procedure is also available for other arrays with reduced scattering grating lobes.

***Index Terms* –** Artificial neural network, metal wall, radar cross-section, scattering grating lobe.

I. INTRODUCTION

With the development of the wave-absorbing material, the radar cross-section (RCS) of a stealth platform is suppressed effectively. The reduction of RCS of antennas still remains to be challenging work. To reduce the RCS of antennas, some effective methods have been proposed. The diffusing of scattering wave based on the metasurface is a remarkable method [1, 2]. The incident wave is diffused by the metasurface covering on the antenna based on the phase cancellation mechanism. Despite that, the diffusing method is not suitable for wide-angle RCS reduction. The absorbing material is also used to reduce RCS [3, 4]. The radiation performance of the antenna, however, is affected because the material also absorbs the radiated waves. One traditional and effective tool to suppress RCS is the frequency selective surface (FSS) covering on antennas. FSS is made as low-RCS shape to diffuse the outbound waves, and the incident inbound wave is absorbed by the loaded antenna, whereas the wave in the neighboring band is also able to penetrate FSS because of the imperfect reflection of the outbound wave. The wave with higher frequency than the inbound wave generates noticeable grating lobes, which highly deteriorate the wide-angle monostatic RCS. It remains a problem for RCS reduction of uniform arrays.

Moreover, the traditional design process is often accompanied by time-consuming full-wave simulations. The artificial neural network (ANN) with the transfer function (TF), as a substitute for the full-wave simulation, has been used for wideband electromagnetic (EM) modeling. By representing the wideband EM response as TF, ANN maps the relationship between the geometric parameters and the response. The trained ANN can obtain the EM response accurately and quickly, and it improves the whole design efficiency.

In this paper, an array whose elements are surrounded by metal walls is proposed for the design of a low RCS array. The array is modeled based on two branch ANNs that independently study the radiation and scattering performances to accelerate the design procedure. In addition, the Fourier series-based TF are used in ANN modeling [5], which has the same order for all samples and fewer coefficient orders than those of the pole-residue-based TF [6], bringing the fast convergency and robustness of the model. The monostatic RCS of the array with no metal wall is also studied for comparison. Simulated results show that the scattering grating lobes are suppressed effectively.

II. DESIGN OF ARRAY WITH LOW-GRATING LOBES

The scattering wave of a periodic structure with the illuminating of a plane wave contains Floquet-Bloch

Submitted On: February 27, 2023
Accepted On: May 16, 2023

https://doi.org/10.13052/2023.ACES.J.380901

modes, as shown in Fig. 1. The Floquet-Bloch waves have transverse wavenumbers as

$$K_s = K_0 \times \sin(\theta) + n \times \frac{2\pi}{P}, n = 0, \pm 1, \pm 2, \ldots, \quad (1)$$

where K_s is the transverse wavenumber of the scattering wave, K_0 is the wavenumber in vacuum, θ is the incident angle, and P is the period of the structure. The transverse wavenumber of the zero-order mode is the same as that of the incident wave. The first high-order mode, i.e., the -1st order mode, is usually the most obvious one, so only n = -1 is considered in this paper. The scattering grating lobe of monostatic RCS appears when the -1st order mode moves in parallel fashion in opposite directions of the incident wave. We have

$$\sin(\theta) = \frac{\lambda_0}{2P}, \quad (2)$$

where λ_0 is the wavelength in vacuum. When $\lambda_0 > 2P$, the -1st order mode is evanescent and the grating lobe is not detectable for the radar.

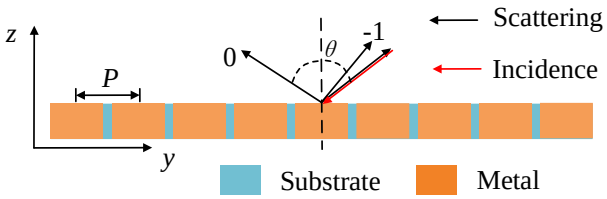

Fig. 1. Periodic structure illuminated by a plane wave.

The common phased array in the stealth platform is a periodic structure. We consider the array operating at 10 GHz as an example, as shown in Fig. 2. The linear array contains 8 elements, and its period is 15 mm. The substrate is Rogers 5880 with a relative dielectric constant of ε_r = 2.2 and a thickness of d = 3 mm.

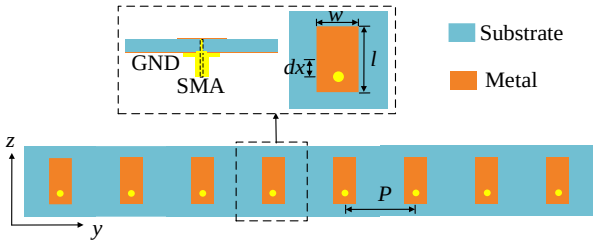

Fig. 2. Structure of the array with no metal wall, where dx = 2.4 mm, w = 6.5 mm, and l = 8.3 mm.

When a plane wave at 12 GHz illuminates the array with an angle of ±56.4°, the monostatic RCS at 12 GHz contains prominent scattering lobes, as shown in Fig. 3. The angle of the -1st scattering mode with P = 15 mm is calculated from (2), as shown in Fig. 4.

To suppress the lobes, metal walls are placed around the array elements, as shown in Fig. 5. The metal walls

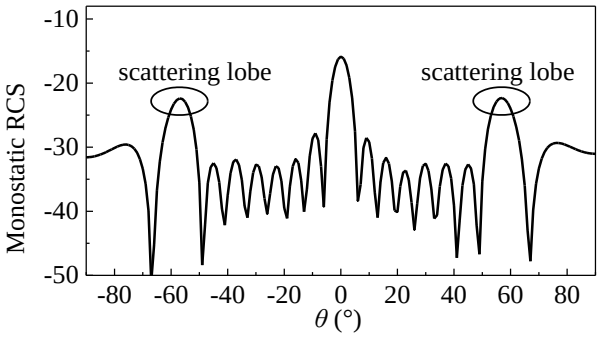

Fig. 3. Monostatic RCS of the array with no metal wall at 12 GHz.

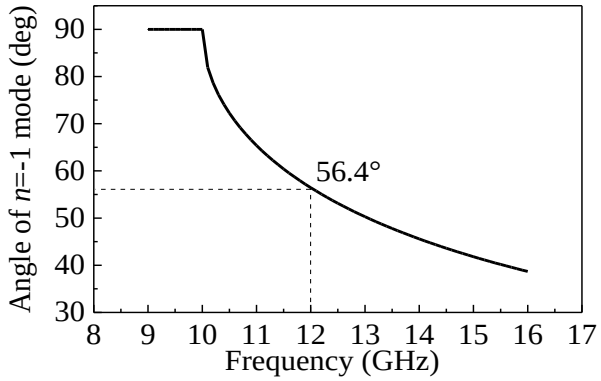

Fig. 4. Angle of the mode with the order of n = -1.

can reduce the scattering grating lobe and maintain the radiation performance of the array.

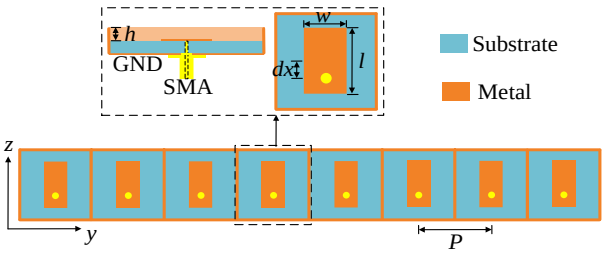

Fig. 5. Structures of the array with metal walls.

From [7], the incident light can be diffracted into the -1st order mode in a broad band by the metallic grating. When a designed metallic grating is placed around the antenna, the -1st order mode can be reduced. Here the metallic walls around the elements work as the metallic gratings. With well-designed metallic walls, the -1st order mode is reduced effectively.

III. OPTIMIZATION DESIGN

The design of the array with metal walls requires numerous full-wave simulations, leading to a time-consuming process. The master-slave boundary and Floquet-Bloch port are used to carry out the element simulation instead of the array simulation. ANN with the Fourier series-based TF is utilized to accelerate the design procedure [5]. The input and output of ANN are the element geometric parameters of $\boldsymbol{x} = [dx, h, l, w]^T$ and the EM response, respectively.

The Fourier series-based TF is written as

$$H(f) = \sum_{k=0}^{N_{\text{order}}} \left(a_k \cos(kq2\pi f) + b_k \cos(kq2\pi f)\right), \quad (3)$$

where N_{order} is the order of TF, a_k and b_k are the TF coefficients, q is the scale factor, and f is the frequency. When $k = 0$, there exists a constant term of a_0. The Fourier series-based TF is used to represent the wideband EM response. With the help of TF, the output of ANN is the coefficients of a_k and b_k instead of the EM response at multiple sampling frequency points. A trained ANN can predict a_k and b_k quickly, and then obtain the wideband EM response from (3). The learning efficiency and generalization of a wideband model can be improved with TF. The Fourier series-based TF only involves real variables and is suitable for real function fitting [5].

With the design of experiment (DOE) method [8], 49 training samples with seven-level and 16 testing samples with four-level defined in Table 1 are obtained from full-wave simulations. The EM response in this paper contains the magnitude of the -1st order Floquet-Bloch mode at 12 GHz when the incident angle is $\pm 56.4^\circ$, and the voltage standing wave ratio (VSWR) of the array is in the range of 9.5-10.5 GHz. Here, we trained two branch ANNs.

Table 1: Definition of training data and testing data for the array

Geometric Parameters	Training Data (49)			Testing Data (16)		
	Min	Max	Step	Min	Max	Step
dx (mm)	1.6	2.4	0.13	1.9	2.2	0.1
h (mm)	1.76	2.64	0.146	1.8	2.1	0.1
l (mm)	7.2	10.8	0.6	8.2	10	0.6
w (mm)	4.8	7.2	0.4	5.4	6.6	0.4

ANN_1, with the Fourier series-based TF, is used to learn the relationship between the geometric parameters and VSWR. The order of the Fourier series-based TF in ANN_1 is chosen as 4 and then the total number of Fourier series coefficients is 9 [5]. From (3), the dimension of ANN_1 output parameters is 9.

ANN_2, with no TF, is used to learn the relationship between the geometric parameters and the magnitude of the -1st order Floquet-Bloch mode. The scattering grating lobe at 12 GHz only appears when the incident angle is equal to $\pm 56.4^\circ$. Because of the axial symmetry of the array, the magnitude of the scattering grating lobe at 56.4° is equal to that at -56.4°. The output of ANN_2 represents the magnitude of the -1st order mode at the incident angle of 56.4°, so TF is not employed for ANN_2 due to the one-dimensional output. The training process of the two branch ANNs is shown in Fig. 6.

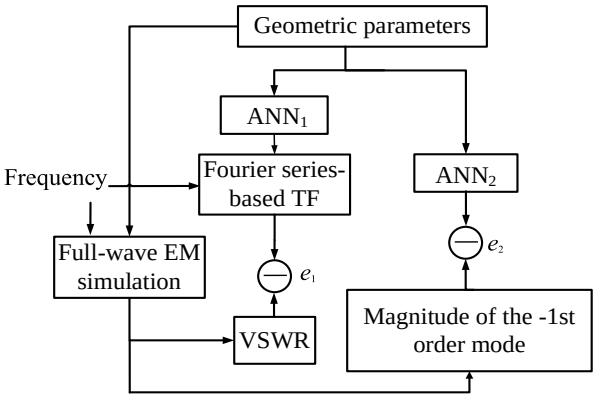

Fig. 6. Training process of the whole ANN model.

The node numbers of the hidden layers of ANN_1 and ANN_2 are determined by the Hecht–Nelson method [9]. When the node number of the input layer is n_{node}, the node number of the hidden layer is $2n_{node} + 1$. The root mean squared errors of e_1 for ANN_1 and e_2 for ANN_2 are provided below.

$$e_1 = \sqrt{\frac{\sum_{i=1}^{N_{\text{sample}}} (VSWR_i^{\text{ANN}} - VSWR_i^{\text{simulation}})^2}{N_{\text{sample}}}}, \quad (4)$$

$$e_2 = \sqrt{\frac{\sum_{i=1}^{N_{\text{sample}}} (mag_i^{\text{ANN}} - mag_i^{\text{simulation}})^2}{N_{\text{sample}}}}, \quad (5)$$

where $VSWR_i^{\text{simulation}}$ is the VSWR calculated from the full-wave simulation of the ith ($1 \leq i \leq N_{sample}$) sample, $VSWR_i^{\text{ANN}}$ is the VSWR calculated from TF whose coefficients of a_k and b_k are obtained by the trained ANN_1, and N_{sample} is the number of the samples. $mag_i^{\text{simulation}}$ is the magnitude of the -1st order Floquet-Bloch mode calculated from the full-wave simulation of the ith sample, and mag_i^{ANN} is obtained from the trained ANN_2.

After the training process, an independent dataset that is never used in training is applied to the testing process. The training and testing errors of ANN_1 are 1.78% and 1.52%, respectively, and the training and testing errors of ANN_2 are 1.04% and 0.93%, respectively. The errors of the ANNs are acceptable. Table 2 summarizes the brief information of the two ANN models.

Table 2: Brief information of two branch ANNs for array modeling

	$\mathbf{ANN}_1$	$\mathbf{ANN}_2$
Input	$\boldsymbol{x}$	$\boldsymbol{x}$
Output	Coefficients of TF (a_k and b_k)	Magnitude of the n=-1 mode
ANN structure	4-9-9	4-9-1
TF	Yes	No
Training error	1.78%	1.04%
Testing error	1.52%	0.93%

After the two ANNs are well trained, the genetic algorithm (GA) is utilized to design the antenna array. GA repeatedly calls the trained ANNs until the optimization objective is achieved, where the optimization objective is the passband of 9.8-10.2 GHz with VSWR < 2 and the magnitude of -1st order mode is small enough. The optimized geometric parameters are $\boldsymbol{x}_{opt}$ = [2.4, 2.5, 8.3, 6.5]^T. The monostatic RCS of the array, calculated by the full-wave simulation with $\boldsymbol{x}_{opt}$, at 12 GHz is shown in Fig. 7. From the figure, the grating lobe is suppressed by 5.8 dB, and the monostatic RCS at the angle of 56.4° is significantly reduced.

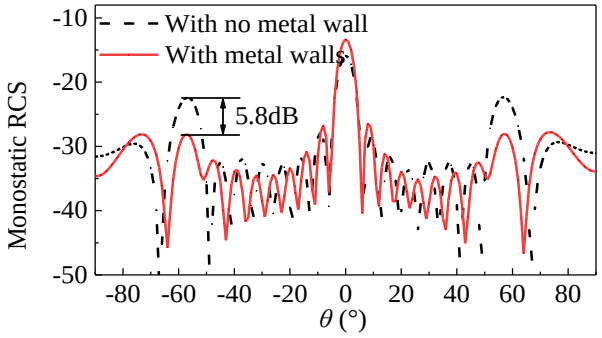

Fig. 7. Monostatic RCS of the array at 12 GHz.

The radiation performance is also considered here. The VSWRs of the optimized arrays with metal walls and without metal wall are provided in Fig. 8. The bandwidth of the array with metal walls is a little narrower than that of the array with no metal wall. Radiation patterns of the array at 10 GHz in the *xoy*-plane are also provided, as shown in Figs. 9 and 10. From Figs. 9 and 10, the gains of the arrays are reduced by 0.9 dB in the normal direction and improved by 1 dB at -50°. The metal wall works as a wide-angle scanning structure, and the change of the radiation performance is acceptable.

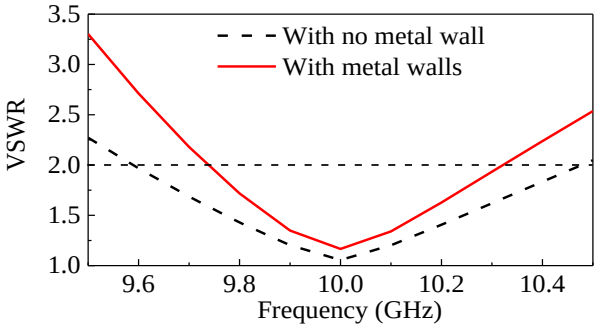

Fig. 8. Simulated VSWR of the center elements.

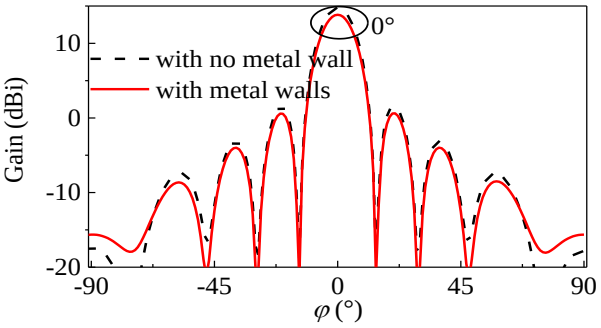

Fig. 9. Radiation patterns of arrays at 10 GHz in the *xoy*-plane with $\varphi = 0°$.

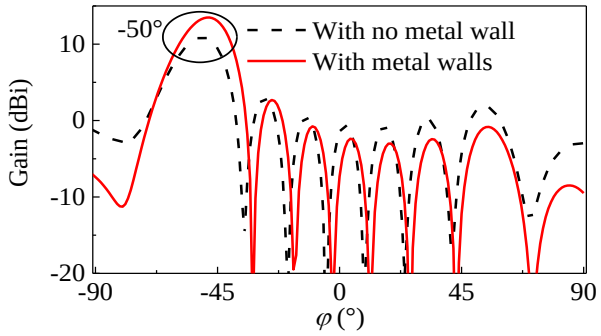

Fig. 10. Radiation patterns of arrays at 10 GHz in the *xoy*-plane with $\varphi = -50°$.

IV. CONCLUSION

In this paper, an array with low scattering grating lobes is proposed. By placing well-designed metallic walls around the array elements, the grating lobe is suppressed and the change of the radiation performance is acceptable. ANN with the Fourier series-based TF, as a substitute for the full-wave simulation, is introduced to accelerate the optimization procedure. The proposed method can also be extended to the application

of two-dimensional (2-D) arrays, and we will study 2-D planar arrays with good radiation/scattering performance in future work.

ACKNOWLEDGMENT

This work was supported by the National Natural Science Foundation of China under Grant 62171093 and by the Sichuan Science and Technology Programs under Grants 2022NSFSC0547 and 2022ZYD0109.

REFERENCES

[1] Y. Gou, Y. Chen, and S. Yang, "Radar cross section reduction of wideband Vivaldy antenna arrays with array-level scattering cancellation," *IEEE Trans. Antenna Propagat.*, vol. 70, no. 8, pp. 6740-6750, Aug. 2022.

[2] W. Zhang, Y. Liu, S. Gong, J. Wang, and Y. Jiang, "Wideband RCS reduction of a slot array antenna using phase gradient metasurface," *IEEE Antennas Wireless Propagat. Lett.*, vol. 17, no. 12, pp. 2193-2197, Dec. 2018.

[3] Y. Q. Li, H. Zhang, Y. Q. Fu, and N. C. Yuan, "RCS reduction of ridged waveguide slot antenna array using EBG radar absorbing material," *IEEE Antenna Wireless Propag. Lett.*, vol. 7, pp. 473-476, 2008.

[4] J. Ren, S. Gong, and W. Jiang, "Low-RCS monopolar patch antenna based on a dual-ring metamaterial absorber," *IEEE Antennas Wireless Propagat. Letters*, vol. 17, no. 1, pp. 102-105, Jan. 2018.

[5] Z. X. Liu, W. Shao, X. Ding, L. Peng, and B. Jiang, "Neural network with Fourier series-based transfer functions for filter modeling," *IEEE Microwave Wireless Compon. Lett.*, vol. 32, no. 7, pp. 823-826, July 2022.

[6] F. Feng, C. Zhang, J. Ma, and Q.-J. Zhang, "Parametric modeling of EM behavior of microwave components using combined neural networks and pole-residue-based transfer functions," *IEEE Trans. Microw. Theory Techn.*, vol. 64, no. 1, pp. 60-77, Jan. 2016.

[7] Z. L. Deng, S. Zhang, and G. P. Wang. "A facile grating approach towards broadband, wide-angle and high-efficiency holographic metasurfaces," *Nanoscale*, vol. 8, no. 3, pp. 1588-1594, 2016.

[8] S. R. Schmidt and R. G. Launsby, *Understanding Industrial Designed Experiments*. Colorado Springs, CO, USA: Air Force Academy, 1992.

[9] R. Hecht-Nielsen, "Kolmogorov's mapping neural network existence theorem," *IEEE Int. Joint Conf. Neural Netw.*, New York, NY, USA, vol. 3, pp. 11-14, June 1987.

Zhi-Xian Liu received the B.S. degree in electronic information science and technology from the China West Normal University, Nanchong, China, in 2019. She is currently pursuing the Ph.D. degree in radio physics in University of Electronic Science and Technology of China (UESTC), Chengdu, China.

Her current research interest includes electromagnetic wave scattering and artificial intelligence.

Wen-Hao Su received the B.S. degree from UESTC, Chengdu, China, in 2021, where he is currently pursuing the master's degree in radio physics.

His current research interests include antenna design and computational electromagnetics.

Sheng-Jun Zhang received the Ph.D. in science from Beijing University of Technology in 2001. From then on he joined the team in National Key Laboratory of Science & Technology on Test Physics and Numerical Mathematics. He is now professor of the laboratory, and his research interest include scattering of EM waves, EM effects of periodic structures such as FSS, PC and gratings, as well as modulation of scattering of materials and interaction of EM waves with plasmas, and IR radiation management.

He has published some papers in journals and conferences, in addition to patents and two books.

Wei Shao received the B.E. degree in electrical engineering from UESTC in 1998, and received M.Sc. and Ph.D. degrees in radio physics from UESTC in 2004 and 2006, respectively.

He joined UESTC in 2007 and is now a professor there. From 2010 to 2011, he was a visiting scholar in the Electromagnetic Communication Laboratory, Pennsylvania State University, State College, PA. From 2012 to 2013, he was a visiting scholar in the Department of Electrical and Electronic Engineering, the University of Hong Kong. His research interests include computational electromagnetics and antenna design.